

## Silica-coated magnetite functionalized with polyaniline for antibacterial and anticandidal treatment

Ayu Sri Wahyuni, Damar Nurwahyu Bima, Choiril Azmiyawati & Adi Darmawan

To cite this article: Ayu Sri Wahyuni, Damar Nurwahyu Bima, Choiril Azmiyawati & Adi Darmawan (2023): Silica-coated magnetite functionalized with polyaniline for antibacterial and anticandidal treatment, International Journal of Polymeric Materials and Polymeric Biomaterials, DOI: [10.1080/00914037.2022.2163637](https://doi.org/10.1080/00914037.2022.2163637)

To link to this article: <https://doi.org/10.1080/00914037.2022.2163637>



Published online: 03 Jan 2023.



Submit your article to this journal [↗](#)



View related articles [↗](#)



View Crossmark data [↗](#)

---



# Silica-coated magnetite functionalized with polyaniline for antibacterial and anticandidal treatment

Ayu Sri Wahyuni , Damar Nurwahyu Bima , Choiril Azmiyawati , and Adi Darmawan 

Department of Chemistry, Diponegoro University, Semarang, Indonesia

## ABSTRACT

This work describes the synthesis of polyaniline/silica-coated magnetite composites (PANI-SMc) for antibacterial and anticandidal applications. PANI-SMc exhibits antimicrobial activity against *Escherichia coli*, *Staphylococcus aureus*, and *Candida albicans*. PANI has a characteristic band at  $1,570\text{ cm}^{-1}$ , corresponds to the  $\text{-C=C-}$  stretching vibrations of quinoid ( $\text{N=Q=N}$ ), and shifted to  $\sim 1,570\text{--}1,620\text{ cm}^{-1}$  in PANI-SMc, indicating imine nitrogen is more involved in the interaction. PANI-SMc shows an amorphous phase, and SMc improves the thermal stability of PANI-SMc. The magnetization of PANI-SMc is lower than SMc; however, it is still firm to be magnetically separated by external magnetic fields. SEM images reveal polyaniline successfully distributed.

## ARTICLE HISTORY

Received 26 July 2022  
Accepted 26 December 2022

## KEYWORDS

Antibacterial; anticandidal;  
polyaniline; silica-coated magnetite

## 1. Introduction

Polyaniline (PANI) is a conducting polymer with immense application in antibacterial and antifungal<sup>[1–4]</sup>. PANI is a highly synthetic polymer that is unique among conjugated polymers because of its electrical conductivity<sup>[5,6]</sup>, high stability in air and solutions of strong acids and alkalis, and easy ways of synthesis<sup>[6]</sup>, low monomer cost<sup>[7]</sup>. Previous studies reported that PANI has a broad range of antimicrobial activity against *Escherichia coli*, *Staphylococcus aureus*, *Pseudomonas aeruginosa*, *Candida albicans*, *Enterococcus faecalis*, and *Campylobacter jejuni*<sup>[3,4]</sup>. The antimicrobial activity of PANI is due to its electrical conductivity, which can mediate contact with negatively charged microbial cell surfaces through electrostatic interactions<sup>[4,8]</sup>.

To increase activity and stability in practical applications, PANI is combined with various support materials. Zhou et al.<sup>[9]</sup> fabricated trimethylsilyl-substituted polyaniline (PSiAn) filler that showed good compatibility and high hydrophobicity in the epoxy matrix. PSiAn inclusion on epoxy coating significantly impacted the barrier property, narrowing the porosity to interrupt the permeation of aggressive substances. Filler, such as titanium dioxide<sup>[10]</sup>, graphene<sup>[11]</sup>, silica<sup>[9,12]</sup>, and magnetite<sup>[6]</sup> had significant advantages due to their development in polymer composites. The interfacial interaction between the polymer chains and the filler is responsible for the synergistic effect of the components in polymer composites<sup>[6]</sup>. It has also been reported that a third phase forms an interface region between the polymer matrix and the filler structures<sup>[13,14]</sup>. This third phase significantly impacts polymer composites' properties, such as biocompatibility<sup>[6]</sup>. This structure offers many advantages in many applications by providing better

properties, including increased antibacterial activity, biocompatibility, and reduced cytotoxicity.<sup>[6]</sup>

On the other hand, magnetite has highly attracted interest in biomedical research applications, such as biosorption<sup>[15]</sup>, biosensing<sup>[16]</sup>, controlled drug delivery<sup>[17]</sup>, tissue engineering<sup>[18]</sup>, and therapeutics agent<sup>[19,20]</sup>, bioseparation<sup>[21]</sup>, magnetic resonance imaging<sup>[22]</sup>, magnetic hyperthermia, and thermoablation<sup>[23]</sup>. These applications require magnetite to have high stability and compatibility and are highly dispersed in various liquid media. One of the main features of magnetite particles is that magnetite can be manipulated and influenced by external magnetic fields to specific areas and target biological entities. However, the use of magnetic nanoparticles is limited because the main disadvantage is agglomeration due to magnetic dipolar attraction. Magnetite is also less stable in dispersion media and lacks affinity for biomolecules, and magnetite undergoes leaching. Hence, adding a coating is a preferable approach to overcome this problem. Several coating materials have been discovered, including surfactant<sup>[24]</sup>, metal<sup>[25]</sup>, and silica<sup>[26]</sup>. Because of its unique surface chemistry, silica is considered one of the most promising alternatives because it prevents magnetite from oxidation and agglomeration and can also be compatible with numerous chemicals and molecules for bioconjugation.

Tetraethyl orthosilicate (TEOS) is generally used as the silane precursor to produce silica-coated magnetite through the Stober method<sup>[27]</sup>. Silane precursor produces orthosilicate acid ( $\text{Si}(\text{OH})_4$ ) through a hydrolysis reaction, and repeated condensation amidst molecules generates siloxane ( $\text{Si-O-Si}$ ) bonds<sup>[28]</sup>. As a result, a silica layer can coat the surface of magnetite. Nevertheless, this typical silica coating method utilizes a mixed solvent consist of

alcohol-water-ammonia and TEOS as silane precursors, resulting in an expensive and complex manufacturing process.

This work presents a facile method for fabricating silica-coated magnetite via sodium silicate ( $\text{Na}_2\text{SiO}_3$ ), commonly used in industries to synthesize  $\text{SiO}_2$  with broader versatility possible than TEOS. Using hydrochloric acid solutions,  $\text{Na}_2\text{SiO}_3$  was titrated at various pH values on the magnetite surfaces to be coated with network structured  $\text{SiO}_2$  and then transformed to  $\text{Si}(\text{OH})_4$ . Silica-coated magnetite composites (SMc) were then functionalized by polyaniline. Therefore, the purpose of this work was to synthesize polyaniline/silica coated-magnetite composites (PANI-SMc), examine the polyaniline surface features and magnetic properties of composites based on the correlation of coating behavior of silica according to pH levels, and evaluate the growth-inhibitory performance of composites against *E. coli*, *S. aureus*, and *C. albicans* microorganisms by the agar well diffusion test. Finally, the PANI-SMc were characterized by Fourier-transform infrared spectroscopy, X-ray diffraction, thermogravimetric analysis, vibrating sample magnetometer, and scanning electron microscopy.

## 2. Methodology

In general, the methodology of this research is summarized in Figure 1.

### 2.1. Materials

Reagents consisted of aniline (Merck), sodium silicate (Merck), ammonium persulfate (Merck), hydrochloric acid (Merck), ethanol (Merck), and natural magnetite powder—technical grade (CV. Satar Unggul Nusa, Indonesia). The bacterial (*E. coli* and *S. aureus*) and fungal (*C. albicans*) strains and reagents for culture media were provided by Biochemistry Laboratory, Chemistry Department, Diponegoro University, Indonesia. All other chemicals used in the study were analytical grade.

### 2.2. Fabrication of silica-coated magnetite with $\text{Na}_2\text{SiO}_3$

The coating process of magnetite was conducted by mixing 2 g of magnetite powder in 40 mL of sodium silicate 10%. The initial pH of the mixture was 12, then 3 M hydrochloric acid solutions were added dropwise until the mixture reached the target pH (9, 8, 7, 6, 5, 4, and 3). The mixture was stirred using a magnetic stirrer for 3 h at a rotational speed of 500 rpm and ambient temperature to produce homogeneous solutions. Then the colloidal suspension can be obtained. As-prepared silica-coated magnetite was aging overnight. The products were filtered and washed several times using distilled water, then dried at 80 °C for 24 h.

### 2.3. Synthesis PANI/silica-coated magnetite composite via in situ oxidative chemical polymerization

PANI/silica-coated magnetite composite preparation has been reported previously<sup>[6]</sup>. The standard procedure was as follows. Aniline 1.83 mL was dissolved in 0.1 mol L<sup>-1</sup> hydrochloric acid 50 mL. Fifty mL of ammonium persulfate (APS) 0.25 mol L<sup>-1</sup> was added to previous solutions. The polymerization medium consisting of silica-coated magnetite, anilinium chloride, and APS was briefly shaken, then left in an ice bath (0–5 °C) for 6 h without stirring. The as-prepared product was collected on a filter, rinsed with ethanol and distilled water, and dried at 60 °C for 12 h.

### 2.4. In vitro antibacterial and anticandida activity of synthesized composite

The agar well diffusion method was performed to assess the zone of inhibition of Gram-positive *S. aureus* and Gram-negative *E. coli* using Nutrient Agar (NA) media. Overnight cultured bacteria were sub-cultured to produce the suspension with a turbidity of 0.5 McFarland ( $1 \times 10^6$  CFU/mL). Thirty  $\mu\text{L}$  of bacteria's suspension were uniformly spread using a sterile cotton swab over the surface of NA plates and left for 10 min to absorb excess moisture. Then 25 mg of synthesized composites and positive control (amoxicillin) were placed onto the 8 mm diameters of wells separately

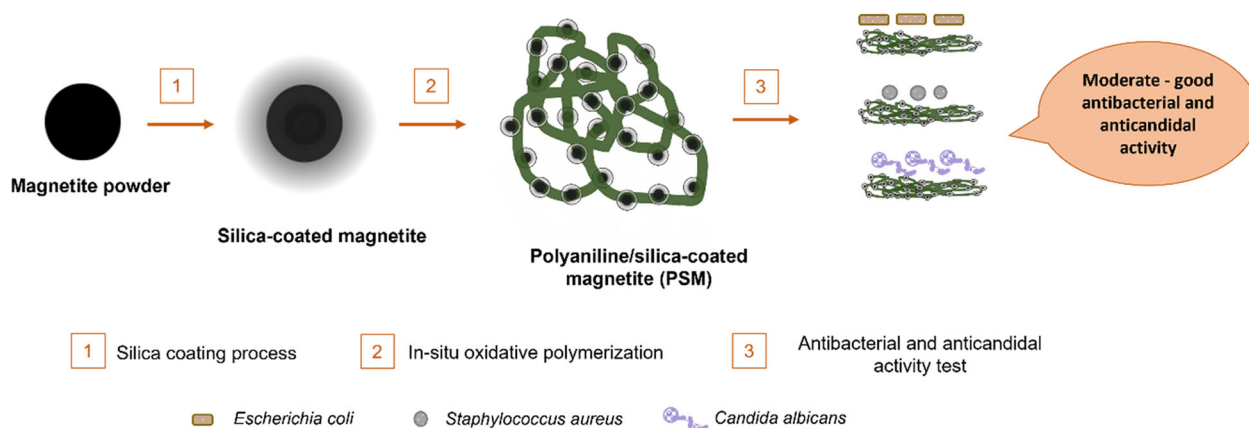


Figure 1. Methodology.

and incubated at 37 °C for 24 h. The zone of inhibition of samples was measured and recorded as antibacterial activity. The same protocol was performed for *C. albicans* using Potato Dextrose Agar (PDA) plates and daktarin as a positive control.

## 2.5. Characterization

The synthesized PANI/Na<sub>2</sub>SiO<sub>3</sub>-magnetite composites were measured using the KBr pellet method using Perkin Elmer Frontier FTIR at 4,000–400 cm<sup>-1</sup>. The crystallinity of the obtained structures was determined by a Shimadzu 7000 model X-ray powder diffractometer with Cu K $\alpha$  radiation. All samples were scanned from 10 to 80° at a 2°/min scan rate. Thermal decomposition profiles of composites were determined using a Mettler Toledo thermal gravimetric analyzer in the temperature range of 25–700 °C at a heating rate of 10 °C/min under a nitrogen atmosphere. The magnetic properties of SMC and PANI-SMC were measured by using a vibrating sample magnetometer (VSM) at room temperature. A scanning electron microscope (Merck Phenom Pro X) was used to determine the surface morphology of composite structures.

## 3. Results and discussion

### 3.1. Fourier transforms infrared spectrophotometric analysis

Figure 2 shows the FTIR spectra of PANI and the PANI-SMC with varied pH levels in the wavenumber region

between 200 and 4,000 cm<sup>-1</sup>. It shows major characteristic peaks at 1,570, 1,490, 1,380, 1,083, and 812 cm<sup>-1</sup>, similar to the standard PANI reported in the literature. PANI spectra show two characteristic bands at 1,570 and 1,490 cm<sup>-1</sup> ascribed to the –C=C– stretching vibrations of quinoid (N=Q=N) and the benzoid (N=B=N) rings, respectively, and represent a clear signature of the polymer backbone<sup>[5,29–31]</sup>. The peak identified at 1083 cm<sup>-1</sup> is probably assigned to the =N<sup>+</sup>–H vibrations (corresponding to a 1,4-disubstituted aromatic ring of PANI)<sup>[29,31]</sup>. This characteristic is associated with electron delocalization in the PANI structure and indicates electrical conductivity. The infrared band around 812 cm<sup>-1</sup> (indicating the head-to-tail coupling within polymer structure) is due to the out-of-plane bending mode of aromatic C–H groups attributed to 1,4-disubstituted aniline units<sup>[30]</sup>.

In comparison, PANI-SMC composites spectra tend to show similar characteristics to PANI. However, PANI-SMC is generally more hygroscopic than PANI, as shown by their broadband at wavenumber around 3,420 cm<sup>-1</sup> with a higher intensity corresponding to (O–H) groups<sup>[7]</sup>. Besides, the peak 1,570 cm<sup>-1</sup> is shifted to a higher wavenumber, about 1,570–1,620 cm<sup>-1</sup>. It indicates that the imine nitrogen is more involved in the interaction<sup>[30,32,33]</sup>. The strong peak in the 1,000–1,200 cm<sup>-1</sup> centered at 1079 cm<sup>-1</sup> is an asymmetric vibration bond of Si–O–Si representing the silica network structure<sup>[27]</sup>. The peak shows the success of the chemical gelation of sodium silicate. The Si–O–Si peak slightly shifts toward smaller wavenumbers (blue shift) with increasing pH content in the sample.

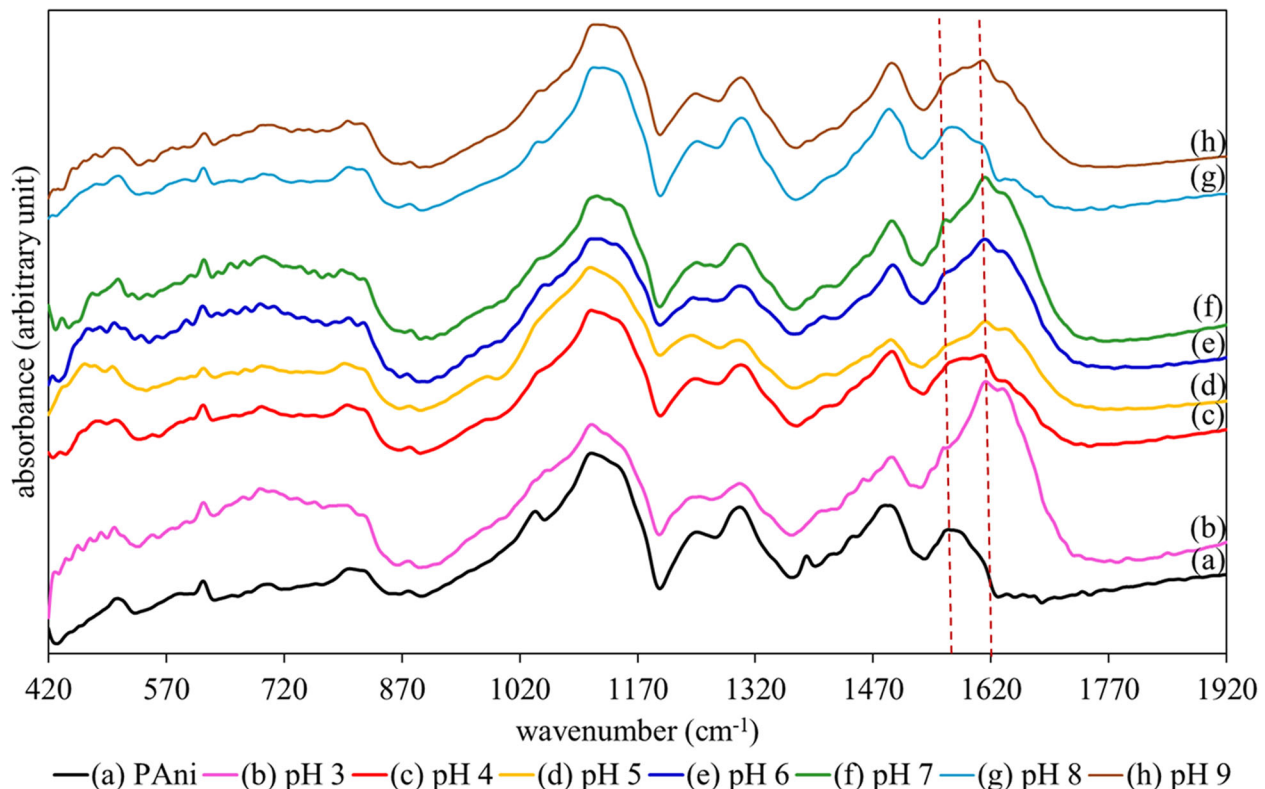


**Figure 2.** FTIR spectra of (a) PANI, (b) PANI-SMC pH 3, (c) PANI-SMC pH 4, (d) PANI-SMC pH 5, (e) PANI-SMC pH 6, (f) PANI-SMC pH 7, (g) PANI-SMC pH 8, and (h) PANI-SMC pH 9.

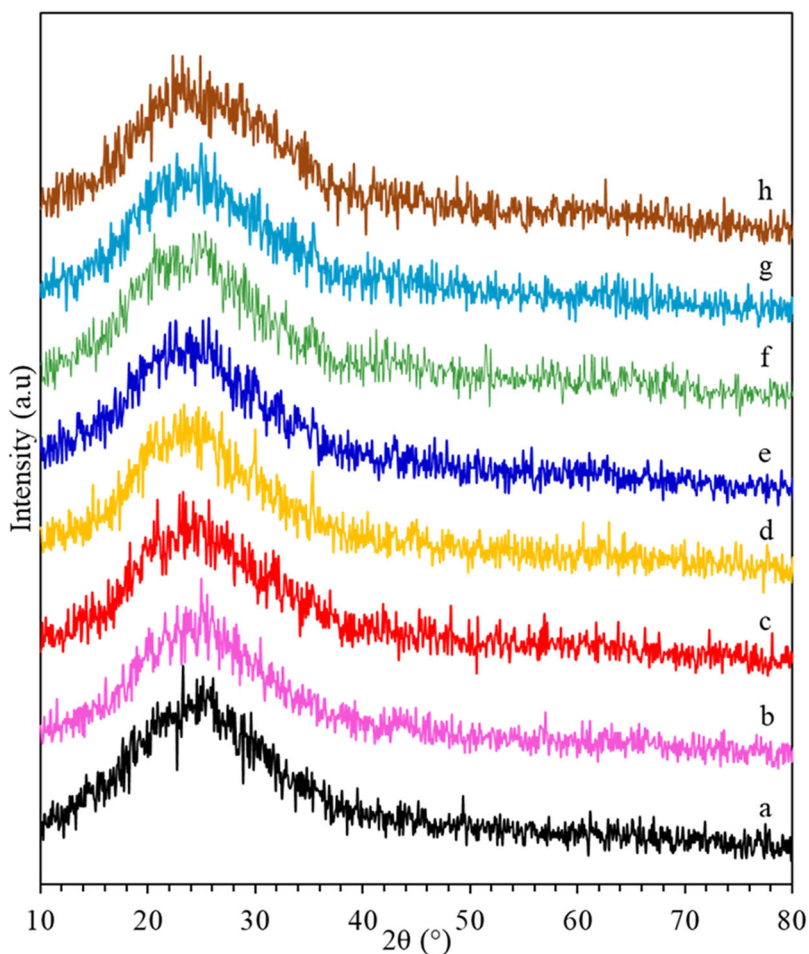


**Figure 3.** XRD patterns of (a) PANI, (b) PANI-SMc pH 3, (c) PANI-SMc pH 4, (d) PANI-SMc pH 5, (e) PANI-SMc pH 6, (f) PANI-SMc pH 7, (g) PANI-SMc pH 8, and (h) PANI-SMc pH 9.

### 3.2. X-ray powder diffraction (XRD)

The presence of silica-magnetite in the dispersed composite was further confirmed by XRD powder studies, as shown in Figure 3. In the case of pristine PANI, the broadband appears at  $2\theta = 24.56^\circ$ , indicating the formation of an amorphous phase in the polymer, which revealed its presence as an amorphous phase in the composites. The XRD pattern of PANI-SMc composites is similar to PANI. Also, the broad peak at  $2\theta = 24.56^\circ$  is observed due to the amorphous nature of  $\text{SiO}_2$  and PANI layers<sup>[34]</sup>. Instead of high-intensity narrower peaks, an X-ray of an amorphous layer is scattered in numerous directions, resulting in a broad bump distributed across a wide range of  $2\theta$ . This broad peak in the PANI-SMc diffraction pattern indicates the low crystallinity of the composite. The inability to detect the magnetite peaks is ascribed to the combined effect of the larger peak width of PANI and the thin silica layer on its surface. This finding confirms that the PANI layer had covered the surface of SMc and did not affect the structure of the SMc embedded in the PANI layer.

### 3.3. Thermogravimetric analysis (TGA)

Thermogravimetric analysis (TGA) of PANI and PANI-SMc were measured in a temperature range of 25–700 °C at a

heating rate of 10 °C/min, as shown in Figure 4A. Thermogravimetric analysis was performed to investigate the thermal properties of the PANI and PANI-SMc and the effect of Si-magnetite content on thermal stability. The thermal degradation of pure PANI (black line) consists of two distinct stages, 50–200 and 300–700 °C, similar to the literature<sup>[35–37]</sup>. At around 50–200 °C, the first stage corresponds to the desorption moisture of polymer (dehydration process), and evaporation of some volatile components and dopant molecules<sup>[6,36,37]</sup>. The desorption of oligomers and deterioration of the polyaniline backbone can be attributed to the second weight loss from 300 to 700 °C<sup>[36,37]</sup>. The thermal degradation profiles of PANI-SM composites tend to be similar to PANI. The first thermal degradation stage of PANI-SMc pH 4, 5, and 7 has a more significant weight loss than PANI, indicating they contained more water and dopant. The opposite occurred at PANI-SMc pH 3, 6, 8, and 9. As seen in the second thermal degradation stage, it is interesting that the presence of silica-coated magnetite pH 4, 5, 7 in composites (PANI-SMc pH 4, 5, 7) strongly prevents the breakdown of the polyaniline backbone because the degradation occurred at around 500 °C instead at 250 °C in polyaniline itself.

A table in Figure 4 shows the weight loss percentage for PANI and PANI-SMc at 700 °C. The presence of silica-coated magnetite content decreased the percent weight, or

in other words, improved the thermal stability of PANI-SM composites. PANI-PSMc pH 8 has the most excellent thermal stability with only 22.33% weight loss along the heating temperature given. The decreases in mass occur along with the appearance of specific peaks on the Differential Thermal Gravimetry (DTG) graph, as shown in Figure 4B. Figure 4B shows the rate of change of mass during the heating process is plotted against temperature. The DTG PANI graph shows a specific curve at around 50 and 300 °C. The curve confirms the thermal decomposition process in the previous PANI TGA graph. The first thermal feature in the DTG

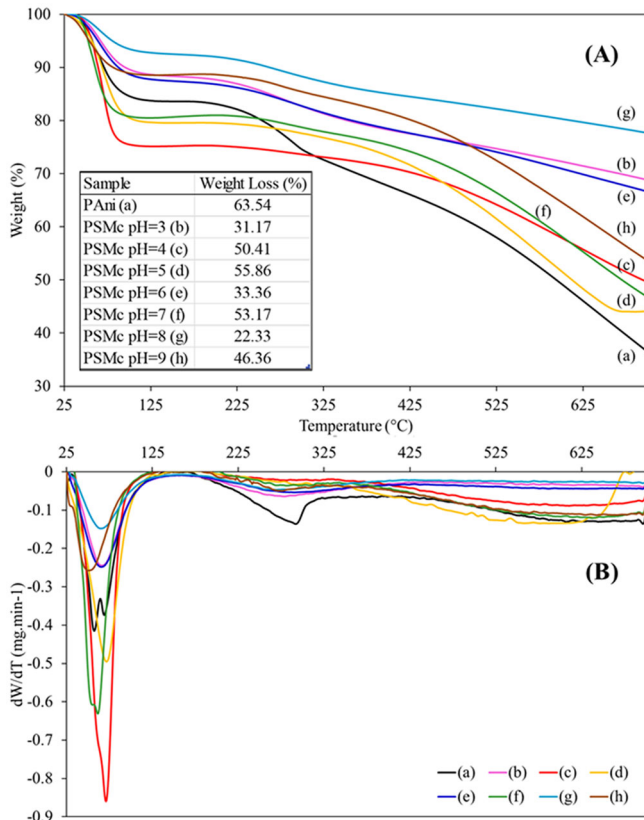


**Figure 4.** (A) TGA and (B) DTG for PANI and PANI-SMc composites at different pH values (a) PANI, (b) PANI-SMc pH 3, (c) PANI-SMc pH 4, (d) PANI-SMc pH 5, (e) PANI-SMc pH 6, (f) PANI-SMc pH 7, (g) PANI-SMc pH 8, and (h) PANI-SMc pH 9.

curves of PANI is ascribed to moisture loss of the polymer, with a maximum breakdown temperature of roughly 57 °C, with a weight loss rate of 0.41 mg/min. DTG curve shows a feature that is not observed in the TGA graph, at around 64 °C, which is probably ascribed to the evaporation of the dopant acid with a maximal degradation temperature of roughly 69 °C, with a degradation rate of 0.37 mg/min. The second feature in the DTG curve of PANI begins at around 300 °C and is linked to a structural deterioration that may result in polyaniline-chain breaking. The maximum temperature of the second stage weight loss occurs at 293 °C with a degradation rate of 0.13 mg/min.

In comparison, the first thermal degradation stage (correspond to desorption moisture and evaporation of dopant) of PANI-SM composites pH 4 (~70 °C) has a most significant weight loss rate of 0.85 mg/min, followed by PANI-SMc pH of 7 at ~61 °C and PANI-SMc pH of 5 at ~73 °C with degradation rate 0.63 and 0.49 mg/min, respectively, higher than PANI. Meanwhile, PANI-SMc pH 3, 6, 8, and 9 have a lower thermal degradation rate than PANI. The second thermal degradation stage of PANI-SM composites has a similar trend to the first, and PANI-SMc pH 8 has the lowest degradation rate, indicating the most stable composites.

### 3.4. Vibrating sample magnetometer (VSM)

The magnetic characteristics of SMc and PANI-SMc were measured at room temperature with a former field of -1 to 1 Tesla using a vibrating sample magnetometer (VSM). Figure 5 represents the sample magnetic hysteresis loop. Adding a polyaniline non-magnetic layer reduces the magnetic saturation ( $M_s$ ) value of the PANI-SM composites so that  $M_s$  of PANI-SMc (around 1.50–2.10  $\text{emu}\cdot\text{g}^{-1}$ ) is lower than SMc. The magnetism of the PANI-SMc, nonetheless, is still strong enough to be magnetically separated by an external magnetic field, enabling the composites to be separated from the reaction solution.

Figure 5 shows the results of the Vibrating Sample Magnetometer (VSM) measurements of pure PANI and PANI-SMc samples at pH variations of 3–9. The hysteresis curve (M-H) indicates that the pure PANI sample behaves

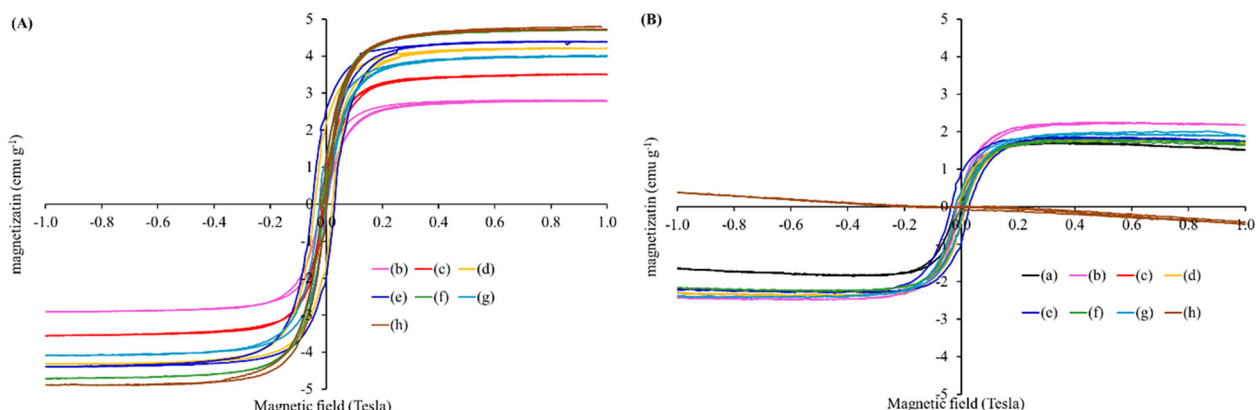


**Figure 5.** Magnetization curves of (A) SMc and (B) PANI-SMc measured by VSM at room temperature.

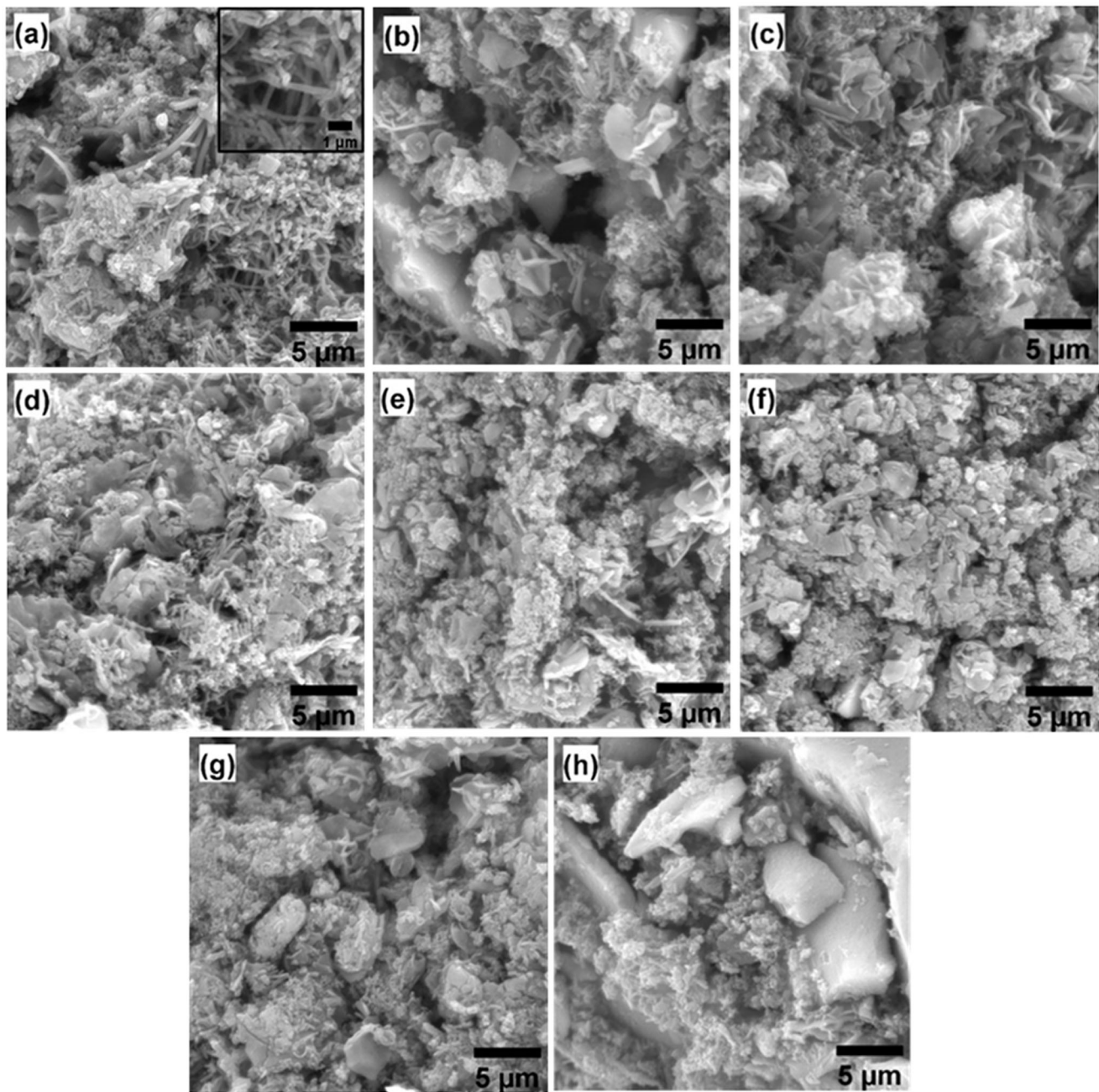


**Figure 6.** SEM images of (a) PANI and PANI-SM composites at different pH: (b) PANI-SM pH 3, (c) PANI-SM pH 4, (d) PANI-SM pH 5, (e) PANI-SM pH 6, (f) PANI-SM pH 7, (g) PANI-SM pH 8, and (h) PANI-SM pH 9.

as diamagnetic. The presence of silica-coated magnetite (SM) composite turned PANI-SM into a ferromagnetic sample. It can be seen that the variation in pH of the silica layer in PANI-SM causes differences in ferromagnetic properties. This is indicated by the sample's difference in saturation ( $M_s$ ) and remanent magnetization ( $M_r$ ). The highest magnetic saturation ( $M_s$ ) of PANI-SM is PANI-SM pH 4,  $2.18 \text{ emu} \cdot \text{g}^{-1}$ , and the lowest is PANI-SM pH 3,  $1.5 \text{ emu} \cdot \text{g}^{-1}$ . Meanwhile, the highest remanence ( $M_r$ ) of PANI-SM is PANI-SM pH 7, and the lowest is PANI-SM pH 3 with remanence of 0.92 and  $0.44 \text{ emu} \cdot \text{g}^{-1}$ .

The ability of PANI-SM to magnetically separate also holds promise for materials recovery. They can be further used in water treatment processes, as mentioned in prior work<sup>[38]</sup>, and thus, material recovery is a crucial strategy for

reducing secondary pollution<sup>[38]</sup>. In the absence of an external magnetic field, the composite can be well dispersed with some motion, indicating that the prepared composite has good dispersibility and magnetic responsibility.

### 3.5. Scanning electron microscope (SEM)

SEM analysis regarding the surface morphology of the composites is presented in Figure 6. PANI itself, as shown in Figure 6a, has a nanotubular shape with a diameter range of 185–365 nm. In contrast, the SEM images of all PANI-SM (Figures 6b–h) reveal a predominant granular morphology. The presence of silica-coated magnetite in PANI-SM generates relatively a slight aggregation on the surface of the

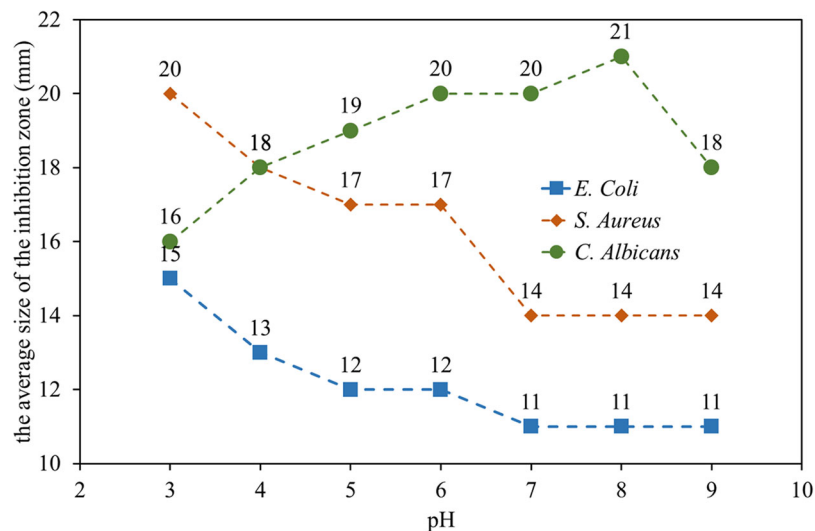


**Figure 7.** The effects of PANI-SM composites pH on growth inhibition of *E. coli*, *S. aureus*, and *C. albicans*.

composites. The aggregation of composites is increased as increased silica layer pH. The SEM image of PANI-SM composites shows that silica-coated magnetite particles have been successfully coated with polyaniline.

### 3.6. Antibacterial and anticandidal activity

The antibacterial and antifungal activity of PANI and PANI-SMc were evaluated against gram-positive bacteria (*S. aureus*), gram-negative bacteria (*E. coli*), and fungi (*C. albicans*) using the agar well diffusion. There are several methods to evaluate the susceptibility of bacteria and fungi. The agar well diffusion test allows rapid identification and reliable measurements of the growth inhibition of microorganisms. The plates were incubated at 37 °C for 24 h, and then the results were evaluated by reading in millimeters the diameter of inhibition of the growth of the microorganisms.

Figure 7 reveals the results of the average zone of inhibition (mm) of PANI-SM composites, PANI, and control against *E. coli*, *S. aureus*, and *C. albicans* microorganisms using the agar well diffusion test. It was observed that PANI has the most robust antimicrobial activities against *E. coli* (19 mm), *S. aureus* (21 mm), and *C. albicans* (28 mm). Microbial susceptibility to PANI is species dependent, meaning that the antimicrobial activity of polyaniline depends on the type of microbe. The results of this study indicate that *C. albicans* is more susceptible to polyaniline than *E. coli* and *S. aureus*. Previous works reported on polyaniline's antibacterial activity. This phenomenon can be explained by (a) the conducting PANI releases the acidic dopant ions, which react with the bacteria cell wall/membrane and then kills it, or (b) both the bacteria and PANI have opposite charge, causing electrostatic adhesion between them so the bacterial cell wall/membrane lysis and leading to the death<sup>[4,38,39]</sup>. It is fascinating that previous research has found that synthetic compounds have significant activity when the inhibition zone is >16 mm, moderate activity when the inhibition zone is 10–16 mm, and weak activity when the inhibition zone is <10 mm.

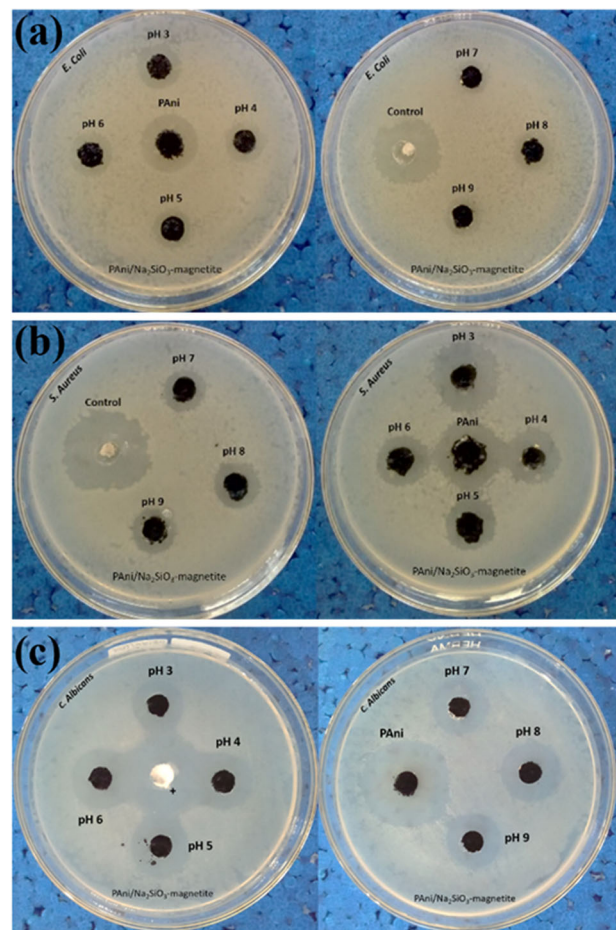


**Figure 8.** Photograph of composites on agar plate (a) *E. coli*, (b) *S. aureus*, and (c) *C. albicans*.

The PANI-SMc showed a lower inhibitory zone than PANI alone Figure 8 shows the effect of pH PANI-SMc on the susceptibility of the microorganisms. The pH of the silica layer in PANI-SMc has a different trend of influence on the activity of antibacterial and anticandidal activities. Antibacterial activity decreased with increasing pH, whereas anticandidal activity increased with increasing pH. pH 3 has

the highest growth inhibition (average zone of inhibition for both *E. coli* and *S. aureus*). As the pH of PANI-SMc increased, the susceptibility of composites decreased. Nevertheless, in neutral to base pH of silica-coated, the PANI-SMc inhibition remained constant at 11 and 14 mm for *E. coli* and *S. aureus*, respectively. By contrast, there was an increase in the average zone of inhibition of PANI-SMc for *C. albicans* as the pH increased and hit a high at pH 8 (21 mm) but turned lower at pH 9 (18 mm). It was proven that different pH levels in the silica coating process affect composites' biological properties. Based on variations in surface magnetite characteristics, the susceptibility of composites is possibly associated with relative electrostatic attractive action. The positive charge of polyaniline on the surface of silica-magnetite acts as a cationic antimicrobial compound that can penetrate the walls and membranes of anionic bacteria. This interferes with cell proliferation and impairs membrane integrity, which ultimately results in cell death<sup>[39]</sup>. The PANI-SMc has higher growth inhibition to *C. albicans* than the two bacteria. Gram-positive bacteria have a single cytoplasmic membrane with a thick multilayer peptidoglycan wall. In contrast, gram-negative bacteria have a more complex cell wall structure with a layer of peptidoglycan between the outer membrane and the cytoplasmic membrane<sup>[39]</sup>. Thereby, the PANI-SMc led to the cell lysis of *S. aureus* (gram-positive) compared to *E. coli* (gram-negative).

#### 4. Conclusions

Polyaniline/silica-coated magnetite composites (PANI-SMc) were produced by the facile method, *in situ* aniline polymerization. The silica layer serves as a component of the ceramic coating, improving the composite's magnetic susceptibility, while polyaniline provides antimicrobial properties. PANI-SMc was shown to have moderate-good antibacterial and anticandidal activity. In addition, PANI-SMc inhibited the growth of microorganisms with an average zone of inhibition in *E. coli* at 12 cm, *S. aureus* at 16 cm, and *C. albicans* at 16 cm. PANI-SMc at acidic pH (pH 3) had the best antibacterial activity compared to neutral and alkaline pH, while PANI-SMc at pH 8 showed the best anticandidal activity.

#### Author contributions

Adi Darmawan: conceptualization, resources, data curation, formal analysis, and supervision. Ayu Sri Wahyuni: investigation, data curation, writing—original draft, and visualization. Damar Nurwahyu Bima: supervision, data curation, and writing—original draft. Choiril Azmiyawati: supervision and writing—review.

#### Disclosure statement

No potential conflict of interest was reported by the author(s).

#### Funding

The author expresses the deepest gratitude for the financial support provided by the Faculty of Science and Mathematics, Diponegoro

University, through Research Funding from Sources of Funds Other Than State Revenue and Expenditure Budget (Non-APBN), 2021 (Number: 2133/UN7.5.8.2/PP/2021) and by the Ministry of Research Technology and Higher Education of the Republic of Indonesia *via* World-Class Research (Number: 521-02/UN7.6.1/PP/2021).

#### ORCID

Ayu Sri Wahyuni  <http://orcid.org/0000-0002-2752-3018>  
 Damar Nurwahyu Bima  <http://orcid.org/0000-0002-3793-8057>  
 Choiril Azmiyawati  <http://orcid.org/0000-0002-4143-9832>  
 Adi Darmawan  <http://orcid.org/0000-0001-5744-5789>

#### References

- [1] Pandiselvi, K.; Thambidurai, S. Synthesis, Characterization, and Antimicrobial Activity of Chitosan–Zinc Oxide/Polyaniline Composites. *Mater. Sci. Semicond. Process.* **2015**, *31*, 573–581. DOI: [10.1016/j.mssp.2014.12.044](https://doi.org/10.1016/j.mssp.2014.12.044).
- [2] Yehgambaram, P.; Prasad, R.; Jakka, V. S.; Aparna, R.; Phani, A. Antifungal Activity of Nanostructured Polyaniline Combined with Fluconazole. *J. Pharm. Res.* **2013**, *6*, 26–31. DOI: [10.1016/j.jopr.2012.11.009](https://doi.org/10.1016/j.jopr.2012.11.009).
- [3] Khan, J. A.; Qasim, M.; Singh, B. R.; Khan, W.; Das, D.; Naqvi, A. H. Polyaniline/CoFe<sub>2</sub>O<sub>4</sub> Nanocomposite Inhibits the Growth of *Candida albicans* 077 by ROS Production. *C. R. Chim.* **2014**, *17*, 91–102. DOI: [10.1016/j.crci.2013.08.006](https://doi.org/10.1016/j.crci.2013.08.006).
- [4] Robertson, J.; Gizdavic-Nikolaidis, M.; Nieuwoudt, M. K.; Swift, S. The Antimicrobial Action of Polyaniline Involves Production of Oxidative Stress While Functionalisation of Polyaniline Introduces Additional Mechanisms. *PeerJ* **2018**, *6*, e5135. DOI: [10.7717/peerj.5135](https://doi.org/10.7717/peerj.5135).
- [5] Kaur, B.; Tanwar, R.; Mandal, U. K. Effect of Nanoparticles Concentration on Thermal, Magnetic and Electrical Properties of Ni<sub>0.5</sub>Zn<sub>0.5</sub>Fe<sub>2</sub>O<sub>4</sub> Based Polyaniline Nanocomposites by *In-Situ* Polymerisation. *Colloids Surf. A Physicochem. Eng. Asp.* **2020**, *599*, 124798. DOI: [10.1016/j.colsurfa.2020.124798](https://doi.org/10.1016/j.colsurfa.2020.124798).
- [6] Lalegül-Ülker, Ö.; Elçin, Y. M. Magnetic and Electrically Conductive Silica-Coated Iron Oxide/Polyaniline Nanocomposites for Biomedical Applications. *Mater. Sci. Eng. C Mater. Biol. Appl.* **2021**, *119*, 111600. DOI: [10.1016/j.msec.2020.111600](https://doi.org/10.1016/j.msec.2020.111600).
- [7] Cha, J. H.; Choi, H.-H.; Jung, Y.-G.; Choi, S.-C.; An, G. S. Novel Synthesis of Core-Shell Structured Fe<sub>3</sub>O<sub>4</sub>@SiO<sub>2</sub> Nanoparticles via Sodium Silicate. *Ceram. Int.* **2020**, *46*, 14384–14390. DOI: [10.1016/j.ceramint.2020.02.233](https://doi.org/10.1016/j.ceramint.2020.02.233).
- [8] Gizdavic-Nikolaidis, M.; Ray, S.; Bennett, J. R.; Eastal, A. J.; Cooney, R. P. Electrospun Functionalized Polyaniline Copolymer-Based Nanofibers with Potential Application in Tissue Engineering. *Macromol. Biosci.* **2010**, *10*, 1424–1431. DOI: [10.1002/mabi.201000237](https://doi.org/10.1002/mabi.201000237).
- [9] Zhou, Z.; Xiao, X.; Wang, W.; Wei, S.; Wang, Y. Enhanced Hydrophobicity and Barrier Property of Anticorrosive Coatings with Silicified Polyaniline Filler. *Colloids Surf. A Physicochem. Eng. Asp.* **2022**, *645*, 128848. DOI: [10.1016/j.colsurfa.2022.128848](https://doi.org/10.1016/j.colsurfa.2022.128848).
- [10] Rezk, A. I.; Bhattarai, D. P.; Park, J.; Park, C. H.; Kim, C. S. Polyaniline-Coated Titanium Oxide Nanoparticles and Simvastatin-Loaded Poly ( $\epsilon$ -Caprolactone) Composite Nanofibers Scaffold for Bone Tissue Regeneration Application. *Colloids Surf. B Biointerfaces* **2020**, *192*, 111007. DOI: [10.1016/j.colsurfb.2020.111007](https://doi.org/10.1016/j.colsurfb.2020.111007).
- [11] Zeeshan, M.; Shah, J.; Jan, M. R.; Iqbal, M. Removal of Bisphenol-A from Aqueous Samples Using Graphene Oxide Assimilated Magnetic Silica Polyaniline Composite. *J. Inorg. Organomet. Polym.* **2021**, *31*, 2073–2082. DOI: [10.1007/s10904-021-01937-y](https://doi.org/10.1007/s10904-021-01937-y).

- [12] Vijayakumar, V.; Khastgir, D. Hybrid Composite Membranes of Chitosan/Sulfonated Polyaniline/Silica as Polymer Electrolyte Membrane for Fuel Cells. *Carbohydr. Polym.* **2018**, *179*, 152–163. DOI: [10.1016/j.carbpol.2017.09.083](https://doi.org/10.1016/j.carbpol.2017.09.083).
- [13] Qiao, R.; Brinson, L. C. Simulation of Interphase Percolation and Gradients in Polymer Nanocomposites. *Compos. Sci. Technol.* **2009**, *69*, 491–499. DOI: [10.1016/j.compscitech.2008.11.022](https://doi.org/10.1016/j.compscitech.2008.11.022).
- [14] Li, H.-X.; Zare, Y.; Rhee, K. Y. The Percolation Threshold for Tensile Strength of Polymer/CNT Nanocomposites Assuming Filler Network and Interphase Regions. *Mater. Chem. Phys.* **2018**, *207*, 76–83. DOI: [10.1016/j.matchemphys.2017.12.053](https://doi.org/10.1016/j.matchemphys.2017.12.053).
- [15] Carvalho Costa, A. W. M.; Guerhardt, F.; Ribeiro Júnior, S. E. R.; Cánovas, G.; Vanale, R. M.; de Freitas Coelho, D.; Ehrhardt, D. D.; Rosa, J. M.; Basile Tambourgi, E.; Curvelo Santana, J. C.; de Souza, R. R. Biosorption of Cr (VI) Using Coconut Fibers from Agro-Industrial Waste Magnetized Using Magnetite Nanoparticles. *Environ. Technol.* **2021**, *42*, 3595–3606. DOI: [10.1080/09593330.2020.1752812](https://doi.org/10.1080/09593330.2020.1752812).
- [16] Jedrzak, A.; Rebiś, T.; Kuznowicz, M.; Jesionowski, T. Bio-Inspired Magnetite/Lignin/Polydopamine-Glucose Oxidase Biosensing Nanoplatform. From Synthesis, via Sensing Assays to Comparison with Others Glucose Testing Techniques. *Int. J. Biol. Macromol.* **2019**, *127*, 677–682. DOI: [10.1016/j.ijbiomac.2019.02.008](https://doi.org/10.1016/j.ijbiomac.2019.02.008).
- [17] Yew, Y. P.; Shameli, K.; Miyake, M.; Khairudin, N. B. B. A.; Mohamad, S. E. B.; Naiki, T.; Lee, K. X. Green Biosynthesis of Superparamagnetic Magnetite Fe<sub>3</sub>O<sub>4</sub> Nanoparticles and Biomedical Applications in Targeted Anticancer Drug Delivery System: A Review. *Arab. J. Chem.* **2020**, *13*, 2287–2308. DOI: [10.1016/j.arabjc.2018.04.013](https://doi.org/10.1016/j.arabjc.2018.04.013).
- [18] Ganapathe, L. S.; Mohamed, M. A.; Mohamad Yunus, R.; Berhanuddin, D. D. Magnetite (Fe<sub>3</sub>O<sub>4</sub>) Nanoparticles in Biomedical Application: From Synthesis to Surface Functionalisation. *Magnetochemistry* **2020**, *6*, 68. DOI: [10.3390/magnetochemistry6040068](https://doi.org/10.3390/magnetochemistry6040068).
- [19] De Toledo, L. D. a S.; Rosseto, H. C.; Bruschi, M. L. Iron Oxide Magnetic Nanoparticles as Antimicrobials for Therapeutics. *Pharm. Dev. Technol.* **2018**, *23*, 316–323. DOI: [10.1080/10837450.2017.1337793](https://doi.org/10.1080/10837450.2017.1337793).
- [20] Mihai, A. D.; Chircov, C.; Grumezescu, A. M.; Holban, A. M. Magnetite Nanoparticles and Essential Oils Systems for Advanced Antibacterial Therapies. *Int. J. Mol. Sci.* **2020**, *21*, 7355. DOI: [10.3390/ijms21197355](https://doi.org/10.3390/ijms21197355).
- [21] Adams, S. A.; Hauser, J. L.; Allen, A. L. C.; Lindquist, K. P.; Ramirez, A. P.; Oliver, S.; Zhang, J. Z. Fe<sub>3</sub>O<sub>4</sub>@SiO<sub>2</sub> Nanoparticles Functionalized with Gold and Poly (Vinylpyrrolidone) for Bio-Separation and Sensing Applications. *ACS Appl. Nano Mater.* **2018**, *1*, 1406–1412. DOI: [10.1021/acsnanm.8b00225](https://doi.org/10.1021/acsnanm.8b00225).
- [22] Soleymani, M.; Khalighfard, S.; Khodayari, S.; Khodayari, H.; Kalhori, M. R.; Hadjighassem, M. R.; Shaterabadi, Z.; Alizadeh, A. M. Effects of Multiple Injections on the Efficacy and Cytotoxicity of Folate-Targeted Magnetite Nanoparticles as Theranostic Agents for MRI Detection and Magnetic Hyperthermia Therapy of Tumor Cells. *Sci. Rep.* **2020**, *10*, 1–14. DOI: [10.1038/s41598-020-58605-3](https://doi.org/10.1038/s41598-020-58605-3).
- [23] Hernández-Hernández, A. A.; Aguirre-Álvarez, G.; Cariño-Cortés, R.; Mendoza-Huizar, L. H.; Jiménez-Alvarado, R. Iron Oxide Nanoparticles: Synthesis, Functionalization, and Applications in Diagnosis and Treatment of Cancer. *Chem. Pap.* **2020**, *74*, 3809–3824. DOI: [10.1007/s11696-020-01229-8](https://doi.org/10.1007/s11696-020-01229-8).
- [24] Dadwal, A.; Joy, P. Influence of Chain Length of Long-Chain Fatty Acid Surfactant on the Thermal Conductivity of Magnetite Nanofluids in a Magnetic Field. *Colloids Surf. A Physicochem. Eng. Asp.* **2018**, *555*, 525–531. DOI: [10.1016/j.colsurfa.2018.07.034](https://doi.org/10.1016/j.colsurfa.2018.07.034).
- [25] Hill, D.; Barron, A. R.; Alexander, S. Comparison of Hydrophobicity and Durability of Functionalized Aluminium Oxide Nanoparticle Coatings with Magnetite Nanoparticles—Links between Morphology and Wettability. *J. Colloid Interface Sci.* **2019**, *555*, 323–330. DOI: [10.1016/j.jcis.2019.07.080](https://doi.org/10.1016/j.jcis.2019.07.080).
- [26] Lakshmi, K.; Rangasamy, R. Synthetic Modification of Silica Coated Magnetite Cored PAMAM Dendrimer to Enrich Branched Aaine Groups and Peripheral Carboxyl Groups for Environmental Remediation. *J. Mol. Struct.* **2021**, *1224*, 129081. DOI: [10.1016/j.molstruc.2020.129081](https://doi.org/10.1016/j.molstruc.2020.129081).
- [27] Darmawan, A.; Smart, S.; Julbe, A.; Diniz Da Costa, J. C. Iron Oxide Silica Derived from Sol-Gel Synthesis. *Materials* **2011**, *4*, 448–456. DOI: [10.3390/ma4020448](https://doi.org/10.3390/ma4020448).
- [28] Yuan, J.; Yang, J.; Ma, H.; Liu, C.; Zhao, C. Hydrothermal Synthesis of Analcime and Hydroxycancrinite from K-Feldspar in Na<sub>2</sub>SiO<sub>3</sub> Solution: Characterization and Reaction Mechanism. *RSC Adv.* **2016**, *6*, 54503–54509. DOI: [10.1039/C6RA08080D](https://doi.org/10.1039/C6RA08080D).
- [29] Chaudhari, H.; Kelkar, D. Investigation of Structure and Electrical Conductivity in Doped Polyaniline. *Polym. Int.* **1997**, *42*, 380–384. DOI: [10.1002/\(SICI\)1097-0126\(199704\)42:4%3C380::AID-PI727%3E3.0.CO;2-F](https://doi.org/10.1002/(SICI)1097-0126(199704)42:4%3C380::AID-PI727%3E3.0.CO;2-F).
- [30] Bhadra, S.; Kim, N. H.; Rhee, K. Y.; Lee, J. H. Preparation of Nanosize Polyaniline by Solid-State Polymerization and Determination of Crystal Structure. *Polym. Int.* **2009**, *58*, 1173–1180. DOI: [10.1002/pi.2646](https://doi.org/10.1002/pi.2646).
- [31] Falletta, E.; Ferretti, A. M.; Mondini, S.; Evangelisti, C.; Capetti, E.; Olivetti, E. S.; Martino, L.; Beatrice, C.; Soares, G.; Pasquale, M.; et al. Size-Dependent Catalytic Effect of Magnetite Nanoparticles in the Synthesis of Tunable Magnetic Polyaniline Nanocomposites. *Chem. Pap.* **2021**, *75*, 5057–5069. DOI: [10.1007/s11696-021-01604-z](https://doi.org/10.1007/s11696-021-01604-z).
- [32] Zhu, J.; Chen, J.; Zhuang, P.; Zhang, Y.; Wang, Y.; Tan, H.; Feng, J.; Yan, W. Efficient Adsorption of Trace Formaldehyde by Polyaniline/TiO<sub>2</sub> Composite at Room Temperature and Mechanism Investigation. *Atmos. Pollut. Res.* **2021**, *12*, 1–11. DOI: [10.1016/j.apr.2020.09.015](https://doi.org/10.1016/j.apr.2020.09.015).
- [33] Abouelsayed, A.; Anis, B.; Eisa, W. H. Terahertz, Infrared, and UV-Vis Spectroscopy Study on Silver@Polyaniline Core@Shell Nanocomposites: Optical and Electronic Properties. *J. Phys. Chem. C* **2020**, *124*, 18243–18256. DOI: [10.1021/acs.jpcc.0c05895](https://doi.org/10.1021/acs.jpcc.0c05895).
- [34] Zhang, S.; Chen, S.; Hu, F.; Xu, R.; Yan, B.; Jiang, M.; Gu, Y.; Yang, F.; Cao, Y. Spray-Processable, Large-Area, Patterned and All-Solid-State Electrochromic Device Based on Silica/Polyaniline Nanocomposites. *Sol. Energy Mater. Sol. Cells* **2019**, *200*, 109951. DOI: [10.1016/j.solmat.2019.109951](https://doi.org/10.1016/j.solmat.2019.109951).
- [35] Moussa, M. A.; Ghoneim, A. M.; Abdel Rehim, M. H.; Khairy, S. A.; Soliman, M. A.; Turky, G. M. Relaxation Dynamic and Electrical Mobility for Poly (Methyl Methacrylate)-Polyaniline Composites. *J. Appl. Polym. Sci.* **2017**, *134*, 45415. DOI: [10.1002/app.45415](https://doi.org/10.1002/app.45415).
- [36] Zailan, F. D.; Chen, R. S.; Shahdan, D.; Ahmad, S. Effect of Conductive Polyaniline in Thermoplastic Natural Rubber Blends on the Mechanical, Thermal Stability, and Electrical Conductivity Properties. *J. Appl. Polym. Sci.* **2019**, *136*, 47527. DOI: [10.1002/app.47527](https://doi.org/10.1002/app.47527).
- [37] Bertuoli, P. T.; Baldissera, A. F.; Zattera, A. J.; Ferreira, C. A.; Aleman, C.; Armelin, E. Polyaniline Coated Core-Shell Polyacrylates: Control of Film Formation and Coating Application for Corrosion Protection. *Prog. Org. Coat.* **2019**, *128*, 40–51. DOI: [10.1016/j.porgcoat.2018.12.007](https://doi.org/10.1016/j.porgcoat.2018.12.007).
- [38] Shi, N.; Guo, X.; Jing, H.; Gong, J.; Sun, C.; Ke, Y. Antibacterial Effect of the Conducting Polyaniline. *J. Mater. Sci. Technol.* **2006**, *22*, 289–290.
- [39] Dhivya, C.; Vandarkuzhali, S. a A.; Radha, N. Antimicrobial Activities of Nanostructured Polyanilines Doped with Aromatic Nitro Compounds. *Arab. J. Chem.* **2019**, *12*, 3785–3798. DOI: [10.1016/j.arabjc.2015.12.005](https://doi.org/10.1016/j.arabjc.2015.12.005).